



Impact of vorticity and viscosity on the hydrodynamic evolution of hot QCD medium

Bhagyarathi Sahoo^{1,a}, Captain R. Singh^{1,b}, Dushmanta Sahu^{1,c}, Raghunath Sahoo^{1,d}, Jan-e Alam^{2,e}

¹ Department of Physics, Indian Institute of Technology Indore, Simrol, Indore 453552, India

² Variable Energy Cyclotron Centre, 1/AF, Bidhan Nagar, Kolkata, India

Received: 26 June 2023 / Accepted: 9 September 2023 / Published online: 27 September 2023
© The Author(s) 2023

Abstract The strongly interacting transient state of quark-gluon plasma (QGP) medium created in ultra-relativistic collisions survives for a duration of a few fm/c. The spacetime evolution of QGP crucially depends on the equation of state (EoS), vorticity, viscosity, and external magnetic field. In the present study, we obtain the lifetime of a vortical QGP fluid within the ambit of relativistic second-order viscous hydrodynamics. We observe that the coupling of vorticity and viscosity significantly increases the lifetime of vortical QGP. The inclusion of a static magnetic field, vorticity, and viscosity makes the evolution slower. However, the static magnetic field slightly decreases the QGP lifetime by accelerating the evolution process for a non-rotating medium. We also report the rate of change of vorticity in the QGP, which will be helpful in studying the behavior of the medium in detail.

1 Introduction

It is reasonable to expect that angular momentum deposition in heavy-ion collisions can trigger a local vortical motion in the overlap region of the colliding species. The initial angular momentum (L_0) generated in a heavy-ion collision is directly proportional to the impact parameter (b) of the collision and the center of mass energy (\sqrt{s}) as $L_0 \propto b\sqrt{s}$ [1]. A fraction of the initial angular momentum is then transferred to the particles that are produced in the collisions. This can manifest as shear along the longitudinal momentum direction, creating vorticity in the system. The ultra-high magnetic field produced by the charged spectators in non-central heavy ion

collisions can also generate vorticity. This generated vorticity, in turn, can affect the evolution of the hot and dense medium. From the global Λ hyperon polarization measurement at Relativistic Heavy Ion Collider (RHIC), it has been estimated that a large vorticity ($\omega = (9 \pm 1) \times 10^{21} \text{ s}^{-1}$) is generated in the system produced in heavy-ion collisions [2]. This makes QGP the most vortical fluid found in nature so far.

There are several sources of vorticity besides the one mentioned above. One such example is the vorticity generated from the jet-like fluctuations in the fireball, which induces a smoke-loop type vortex around a fast-moving particle [3]. This vorticity, however, does not contribute to global hyperon polarization. Another source of vorticity is the inhomogeneous expansion of the fireball. Due to the anisotropic flows in the transverse plane, a quadrupole pattern of the longitudinal vorticity along the beam direction is produced [4–10]. On the other hand, the inhomogeneous transverse expansion produces transverse vorticity that circles the longitudinal axis. In addition, another source of vorticity can be due to the Einstein-de Haas effect [11], where a strong magnetic field created by the fast-moving spectators magnetizes the QCD matter, and due to the magnetization, a rotation is induced. This leads to the generation of vorticity along the direction of the magnetic field. This effect is opposite to the Barnett effect, where a chargeless rotating system creates a non-zero magnetization [12].

Vorticity formation in the ultra-relativistic heavy-ion collision has been studied by using hydrodynamic models such as ECHO-QGP, PICR, vHLLE, MUSIC, 3-FD, CLVisc in (3+1) dimensional model [13–18]. Event generators, such as AMPT, UrQMD, and HIJING, have also been used to estimate kinematic and thermal vorticity [5–7, 19–22]. Moreover, the non-zero local vorticity can help us to probe the chiral vortical effect (CVE), which is a non-trivial consequence of topological quantum chromodynamics [23, 24].

^a e-mail: Bhagyarathi.Sahoo@cern.ch

^b e-mail: captainriturajsingh@gmail.com

^c e-mail: Dushmanta.Sahu@cern.ch

^d e-mail: Raghunath.Sahoo@cern.ch (corresponding author)

^e e-mail: jane@vecc.ac.in

This effect is the vortical analog of the chiral magnetic effect (CME) [25, 26] and chiral separation effect (CSE) [27, 28]. It represents the vector and axial currents generation along the vorticity [29–32]. CVE is extremely important because it induces baryon charge separation along the direction of vorticity, which can be experimentally probed by two-particle correlations [33].

Relativistic hydrodynamics govern the evolution of matter produced in ultra-relativistic collisions. Thus, relativistic hydrodynamics models with finite viscous correction become very useful in understanding the spacetime evolution of the system created in such collisions. From the AdS/CFT correspondence, the lower limit of shear viscosity (η) to entropy density(s) ratio has been predicted, which is known as the KSS bound, given by $\eta/s \simeq 1/4\pi$ [34]. Hydrodynamic models with $\eta/s \simeq 0.2$ explain the elliptic flow results from the RHIC experiments very well [35]. Moreover, as observed in some recent studies [36], viscosity can generate some finite vorticity in the medium, even if initial vorticity is absent a priori. This makes the evolution dynamics of the viscous medium fascinating.

In the non-relativistic domain, the vorticity is defined as the curl of the velocity (ω) field of the fluid as,

$$\boldsymbol{\omega} = \frac{1}{2} \nabla \times \mathbf{v}$$

Since high energy heavy-ion collision is a relativistic system, the generalized form of vorticity which is mostly used in the relativistic domain is thermal vorticity, which is defined as,

$$\omega_{\mu\nu} = -\frac{1}{2} (\partial_\mu \beta_\nu - \partial_\nu \beta_\mu)$$

where $\beta_\mu = \frac{u_\mu}{T}$, with u_μ being the four-velocity of the fluid and T is the temperature. Apart from thermal vorticity, there are several other kinds of vorticity; such as kinematic vorticity, temperature vorticity, and enthalpy vorticity in relativistic hydrodynamics, which have various implications as discussed in Refs. [13, 14, 37].

In Ref. [38], the authors have used an ideal equation of state and estimated the time evolution of non-relativistic vorticity. They show that vorticity decreases as the system evolves with time. As mentioned earlier, the finite viscosity and vorticity of a rotational viscous fluid originate from several sources. In the present work, we study the evolution of QGP using second-order viscous hydrodynamics in the presence of vorticity. The effect of static magnetic field on evolution has also been included here. We obtain a set of coupled differential equations describing the evolution of the system. These coupled equations together describe the time evolution of temperature, viscosity, and vorticity.

This paper is organized as follows. In Sect. 2, we briefly discuss the effects of viscosity and vorticity on the temper-

ature through a set of non-linear coupled differential equations. In Sect. 3, we discuss the results obtained from hydrodynamic equations, which describe the evolution of temperature, viscosity, and vorticity and how much it is sensitive to initial hydrodynamic conditions. Finally, we summarize the essential findings in Sect. 4.

2 Evolution of the system

We first discuss the temperature profile for a simple relativistic ideal fluid. Secondly, we discuss temperature and viscosity evolution with proper time for a second-order relativistic viscous fluid. The following subsection discusses the evolution of temperature, viscosity, and vorticity for a relativistic rotational viscous fluid. Finally, we discuss the temperature, viscosity, and vorticity evolution of a rotating viscous fluid in a static magnetic field.

2.1 Ideal fluid

For an ideal fluid, the energy-momentum tensor ($T^{\mu\nu}$) does not contain a gradient of the hydrodynamic fields. This is called a 0th order hydrodynamic model. The energy-momentum tensor for relativistic ideal hydrodynamics is,

$$T_{Ideal}^{\mu\nu} = (\epsilon + P) u^\mu u^\nu - g^{\mu\nu} P \quad (1)$$

where ϵ is energy density, P is pressure, $u^\mu = \gamma(1, \mathbf{v})$ is the four-velocity vector, with $\gamma = \frac{1}{\sqrt{1-\mathbf{v}^2}}$ being the Lorentz factor, and $g^{\mu\nu} = diag(1, -1, -1, -1)$ is the metric tensor. The conservation of energy-momentum (in absences of external field) is given by,

$$\partial_\mu T^{\mu\nu} = 0 \quad (2)$$

Projecting Eq. (2) in the direction parallel to the fluid velocity, we get;

$$u_\nu \partial_\mu T^{\mu\nu} = 0 \quad (3)$$

Simplification of Eq. (3) leads to,

$$\partial_\mu ((\epsilon + P) u^\mu) = u_\nu g^{\mu\nu} \partial_\mu P \quad (4)$$

Using the relation $D \equiv u^\mu \partial_\mu = \gamma \frac{d}{d\tau}$ in Eq. (4), produces the dissipation rate for energy density,

$$\frac{d\epsilon}{d\tau} = -\frac{1}{\gamma} (\epsilon + P) \partial_\mu u^\mu \quad (5)$$

For this study, we use a simple equation of state (EoS) describing an ideal plasma of massless u, d, s quarks, and gluons. The pressure is given by $P = \epsilon/3 = aT^4$ with zero

baryon chemical potential, where a is the constant, defined as [39–41]

$$a = \frac{\pi^2}{90} \left[16 + \frac{21}{2} N_f \right]$$

where $N_f = 3$, is the number of flavours. Using the EoS mentioned above, the equation governing the cooling rate can be obtained as,

$$\frac{dT}{d\tau} = -\frac{T}{3\gamma} \partial_\mu u^\mu \quad (6)$$

Equation (6) represents the cooling rate in 0^{th} order hydrodynamics or for ideal fluid.

2.2 Viscous fluid

The viscosity in a medium originates due to the velocity gradient between fluid cells which slows down the flow. Therefore, considering QGP as a viscous fluid modifies the medium evolution. The dissipative term ($\Pi^{\mu\nu}$) needs to be added to the energy-momentum tensor ($T_{Ideal}^{\mu\nu}$) representing the ideal fluid such that the total energy-momentum tensor is given by:

$$T^{\mu\nu} = T_{Ideal}^{\mu\nu} + \Pi^{\mu\nu} \quad (7)$$

where $\Pi^{\mu\nu}$ is the viscous stress tensor, expressed as,

$$\Pi^{\mu\nu} = \pi^{\mu\nu} + \Delta^{\mu\nu} \Pi$$

where $\Delta^{\mu\nu} = g^{\mu\nu} - u^\mu u^\nu$ is the projection operator, such that $\Delta^{\mu\nu} u_\nu = 0$. The $\Pi^{\mu\nu}$ contains two parts; $\pi^{\mu\nu}$ accounts for the shear viscosity, and $\Delta^{\mu\nu} \Pi$ accounts for the bulk viscosity. For conformal fluids, the bulk viscous pressure does not contribute ($\Pi = 0$) [42]. For first-order hydrodynamic theory, the $\pi^{\mu\nu}$ has the form;

$$\pi^{\mu\nu} = \eta \nabla^{<\mu} u^{\nu>} \quad (8)$$

where η is the shear viscosity, with:

$$\nabla^{<\mu} u^{\nu>} \equiv 2 \nabla^{(\mu} u^{\nu)} - \frac{2}{3} \Delta^{\mu\nu} \nabla^\alpha u_\alpha$$

where $\nabla^{(\mu} u^{\nu)}$ is defined as $A^{(\mu} B^{\nu)} = \frac{1}{2} (A^\mu B^\nu + A^\nu B^\mu)$.

For second-order hydrodynamic theory, the $T^{\mu\nu}$ contains both the first and second-order gradient of the hydrodynamic fields. In Müller–Israel–Stewart (MIS) second-order theory, the $\pi^{\mu\nu}$ is given by [43],

$$\pi^{\mu\nu} = \eta \nabla^{<\mu} u^{\nu>} + \tau_\pi \left[\Delta_\alpha^\mu \Delta_\beta^\nu D\pi^{\alpha\beta} \dots \right] + O(\delta^2) \quad (9)$$

where τ_π is the relaxation time. Inclusion of the viscous term in energy density evolution changes Eq. (5) to the following

form [39–41];

$$\frac{d\epsilon}{d\tau} = -\frac{1}{\gamma} (\epsilon + P - \Phi) \partial_\mu u^\mu \quad (10)$$

Here $\Phi = \pi^{00} - \pi^{zz}$ is the difference between temporal and spatial components of the shear viscosity tensor representing the viscous term.

For first-order theory, the viscous shear term $\Phi = \frac{4\eta}{3\tau}$. The second-order MIS relaxation equation using Grad's 14 moments methods for shear viscosity has the following form [39–41];

$$D\pi^{\mu\nu} = -\frac{1}{\tau_\pi} \pi^{\mu\nu} - \frac{1}{2\beta_2} \pi^{\mu\nu} \left[\beta_2 \theta + TD \left(\frac{\beta_2}{T} \right) \right] + \frac{1}{\beta_2} \nabla^{<\mu} u^{\nu>} \quad (11)$$

where $\theta \equiv \partial_\mu u^\mu$ represents the expansion of the system, $\tau_\pi = 2\eta\beta_2$ is the relaxation time, β_2 is the relaxation coefficient given as; $\beta_2 = 3/4P$. Here we take shear viscosity $\eta = bT^3$, where b is defined as;

$$b = (1 + 1.70N_f) \frac{0.342}{(1 + N_f/6)\alpha_s^2 \ln(\alpha_s^{-1})}$$

where $\alpha_s = 0.5$, is the strong coupling constant.

Now, the evolution of shear viscosity can be obtained from the Eq. (11) as a viscous shear tensor,

$$\frac{d\Phi}{d\tau} = -\frac{\Phi}{\gamma\tau_\pi} - \frac{\Phi}{2\gamma} \left(\partial_\mu u^\mu + \frac{\gamma}{\beta_2} T \frac{d}{d\tau} \left(\frac{\beta_2}{T} \right) \right) + \frac{1}{\gamma\beta_2} (\nabla^{<0} u^{0>} - \nabla^{<z} u^{z>}) \quad (12)$$

Using the equation of state, $P = \epsilon/3 = aT^4$ to the Eqs. (10) and (12), we have,

$$\frac{dT}{d\tau} = -\frac{1}{\gamma} \left(\frac{T}{3} - \frac{T^{-3}\Phi}{12a} \right) \partial_\mu u^\mu \quad (13)$$

$$\frac{d\Phi}{d\tau} = -\frac{2aT\Phi}{3b\gamma} - \frac{\Phi}{2\gamma} \left(\partial_\mu u^\mu - \frac{5\gamma}{T} \frac{dT}{d\tau} \right) + \frac{4aT^4}{3\gamma} (\nabla^{<0} u^{0>} - \nabla^{<z} u^{z>}) \quad (14)$$

Thus, Eqs. (13) and (14) represent the space-time evolution of temperature and viscous term (Φ) with the proper time, which cumulatively affects the temperature evolution in the second-order theory. Furthermore, by putting $\Phi = 0$ in Eqs. (13) and (14), one gets the equation of motion for the ideal fluid.

2.3 Rotational viscous fluid

Next, we consider a viscous medium with non-zero vorticity, which can couple with the spin of the particles and gives rise to spin polarization in the system. Here spin polarization

tensor is obtained using a tensor decomposition with the help of Ref. [44]. The antisymmetric spin polarization tensor is given as;

$$\omega_{\mu\nu} = k_\mu u_\nu - k_\nu u_\mu + \epsilon_{\mu\nu\alpha\beta} u^\alpha \omega^\beta \quad (15)$$

where, k_μ and ω_μ are defined in terms of spin polarization tensor;

$$k_\mu = \omega_{\mu\nu} u^\nu, \quad \omega_\mu = \frac{1}{2} \epsilon_{\mu\nu\alpha\beta} \omega^{\nu\alpha} u^\beta \quad (16)$$

To hold the relation $k^\mu u_\mu = \omega^\mu u_\mu = 0$, the ω_μ and k_μ are set to orthogonal to the fluid velocity u_μ . Here $\epsilon_{\mu\nu\alpha\beta}$ is the Levi Civita antisymmetric four tensor, $\epsilon^{0123} = -\epsilon_{0123} = 1$. Considering the rotation in the $x-z$ plane, i.e. $\omega_\mu = (0, 0, \omega, 0)$, one needs to solve Eqs. (15) and (16) self-consistently to obtain the spin polarization tensor, $\omega_{\mu\nu}$;

$$\omega_{\mu\nu} = \begin{bmatrix} 0 & 0 & 0 & 0 \\ 0 & 0 & 0 & \frac{\omega}{T} \\ 0 & 0 & 0 & 0 \\ 0 & -\frac{\omega}{T} & 0 & 0 \end{bmatrix} \quad (17)$$

For this work, we have considered the velocity profile $u^\mu = \gamma(1, v_x, 0, v_z)$. The velocity profile is chosen in such a way that the transverse component of velocity depends upon the longitudinal component and the longitudinal component of velocity develops a transverse component. The chosen velocity profiles are [38];

$$v_x = \frac{\omega z}{2} \quad (18)$$

$$v_z = \frac{z}{\tau} - \frac{\omega x}{2} \quad (19)$$

where x and z are the position coordinates. Here it is important to note that vorticity is the cause of inducing the velocity along x -direction, i.e., v_x . We have introduced the vorticity into the system through the modified Euler's thermodynamic relation [38,44,45], we have;

$$\epsilon + P = Ts + \mu n + \Omega w \quad (20)$$

Here, Ω is the chemical potential corresponding to rotation, and w is the rotation density. Further, one can define $\Omega = \frac{T}{2\sqrt{2}} \sqrt{\omega_{\mu\nu} \omega^{\mu\nu}}$ and $w = 4 \cosh(\xi) n_0$, where $\xi = \frac{\omega}{2T}$ and $n_0 = \frac{T^3}{\pi^2}$ is the number density of the particles in the massless limit. Thus, the rotation density becomes $w = 4 \frac{T^3}{\pi^2} \cosh\left(\frac{\omega}{2T}\right)$ [38].

Thus, taking all the above inputs at zero baryonic chemical potential, Eq. (20) can be modified as,

$$\epsilon + P = Ts + \frac{2\omega T^3}{\pi^2} \cosh\left(\frac{\omega}{2T}\right) \quad (21)$$

Under the ideal limit, $\epsilon = 3P$. Hence the above equation becomes,

$$\epsilon = \frac{3}{4} \left[Ts + \frac{2\omega T^3}{\pi^2} \cosh\left(\frac{\omega}{2T}\right) \right] \quad (22)$$

Differentiating the above equation with respect to proper time τ ,

$$\frac{d\epsilon}{d\tau} = \frac{3}{4} \left[\frac{T ds}{d\tau} + \frac{s dT}{d\tau} + \frac{2}{\pi^2} \frac{d}{d\tau} \left(\omega T^3 \cosh\left(\frac{\omega}{2T}\right) \right) \right] \quad (23)$$

We use the standard form of entropy, $s = c + dT^3$, where c and d are constants to obtain,

$$\frac{d\epsilon}{d\tau} = \frac{3}{4} \left[\left(s + 3dT^3 + \frac{2F}{\pi^2} \right) \frac{dT}{d\tau} + \frac{2G}{\pi^2} \frac{d\omega}{d\tau} \right] \quad (24)$$

where, $F = 3T^2 \omega \cosh\left(\frac{\omega}{2T}\right) - \frac{1}{2} \omega^2 T \sinh\left(\frac{\omega}{2T}\right)$ and $G = T^3 \cosh\left(\frac{\omega}{2T}\right) + \frac{1}{2} \omega T^2 \sinh\left(\frac{\omega}{2T}\right)$. Now, using Eq. (21) in Eq. (10), we get,

$$\frac{d\epsilon}{d\tau} = -\frac{1}{\gamma} \left(Ts + \frac{2\omega T^3}{\pi^2} \cosh\left(\frac{\omega}{2T}\right) - \Phi \right) \partial_\mu u^\mu \quad (25)$$

Comparing Eqs. (24) and (25) we get,

$$\begin{aligned} \frac{d\omega}{d\tau} = & \frac{-\pi^2}{2G} \left[\frac{4T}{3\gamma} \left(s + \frac{2T^2 \omega}{\pi^2} \cosh\left(\frac{\omega}{2T}\right) - \frac{\Phi}{T} \right) \partial_\mu u^\mu \right. \\ & \left. + \left(s + 3dT^3 + \frac{2F}{\pi^2} \right) \frac{dT}{d\tau} \right] \end{aligned} \quad (26)$$

The temperature evolution equation can be obtained from the energy evolution Eq. (25) using the aforementioned EoS. The modified temperature cooling rate is presented as;

$$\frac{dT}{d\tau} = \frac{1}{\gamma} \left[-\frac{T}{3} \left(1 + \frac{2\omega T^2}{s\pi^2} \cosh\left(\frac{\omega}{2T}\right) \right) + \frac{\Phi T^{-3}}{12a} \right] \partial_\mu u^\mu \quad (27)$$

Thus, vorticity can also generate viscosity in the medium. In this work, we have taken the direct contribution of vorticity in viscosity evolution through MIS equation [41]. Here we have incorporated the viscous and vorticity coupling term $\pi_\alpha^{(\mu} \omega^{\nu)\alpha}$ through a second order transport coefficient λ [46].

$$\begin{aligned} D\pi^{\mu\nu} = & -\frac{1}{\tau_\pi} \pi^{\mu\nu} - \frac{1}{2\beta_2} \pi^{\mu\nu} \left[\beta_2 \theta + TD \left(\frac{\beta_2}{T} \right) \right] \\ & + \frac{1}{\beta_2} \nabla^{<\mu} u^{\nu>} + \lambda \pi_\alpha^{(\mu} \omega^{\nu)\alpha} \end{aligned} \quad (28)$$

Starting with Eq. (21), the coupling of shear stress tensor with vorticity can be written as:

$$\frac{d\Phi}{d\tau} = -\frac{2aT\Phi}{3b\gamma} - \frac{\Phi}{2\gamma} \left(\partial_\mu u^\mu - \frac{5\gamma}{T} \frac{dT}{d\tau} \right)$$

$$+ \frac{4aT^4}{3\tau\gamma} (\nabla^{<0} u^{0>} - \nabla^{<z} u^{z>}) - \frac{\omega\Phi}{\gamma T\tau} \quad (29)$$

In the present context the detailed expressions for $u^\mu \partial_\mu$, $\partial_\mu u^\mu$, $\nabla^{<0} u^{0>} - \nabla^{<z} u^{z>}$, and $\pi_\alpha^{(\mu} \omega^{\nu)\alpha}$ are derived in Appendix (A), (B), (C) and (D), respectively. Finally, we get the three non-linear coupled differential Eqs. (26), (27), and (29) describing the medium evolution in terms of vorticity, temperature, and viscosity, respectively. If we take $\omega = 0$, then it reduces to the second-order viscous hydrodynamics, and further, if we take $\Phi = 0$, then it gives us a solution corresponding to the ideal fluid.

2.4 Rotational viscous fluid in the presence of magnetic field

Next, we consider the evolution of charged fluid rotating in a viscous medium in the presence of the magnetic field. In such a case, the energy-momentum tensor for rotating, viscous and magnetized fluid is given by [47,48];

$$T^{\mu\nu} = \left(\epsilon + P + B^2 \right) u^\mu u^\nu - g^{\mu\nu} \left(P + \frac{B^2}{2} \right) - B^\mu B^\nu + \pi^{\mu\nu} \quad (30)$$

where $B^\mu = \frac{1}{2}\epsilon^{\mu\nu\alpha\beta} F_{\nu\alpha} u_\beta$ is the magnetic field in the fluid, $F_{\nu\alpha}$ is the field strength tensor. The magnetic field four vector B^μ is space-like four vector with modulus $B^\mu B_\mu = -1$ and orthogonal to u^μ that is $B^\mu u_\mu = 0$, where $B = |\mathbf{B}|$, and $|\mathbf{B}|$ is the magnetic three vector.

The energy density evolution equation for a viscous medium in the presence of a magnetic field can be obtained from the energy-momentum conservation, Eq. (2) is given by [47,49];

$$\frac{d\epsilon}{d\tau} = -\frac{1}{\gamma} \left(\epsilon + P + B^2 - \Phi \right) \partial_\mu u^\mu - B \frac{dB}{d\tau} \quad (31)$$

Proceeding in the same way as Sect. 2.3, using the modified Euler equation $\epsilon + P = Ts + \mu n + \Omega w + eBM$, where $M = \chi_m B$ is the magnetization of the fluid, χ_m being the magnetic susceptibility, we have;

$$\frac{d\omega}{d\tau} = \frac{-\pi^2}{2G} \left[\left(s + 3dT^3 + \frac{2F}{\pi^2} \right) \frac{dT}{d\tau} + \left(\frac{4}{3} + 2e\chi_m \right) B \frac{dB}{d\tau} + \frac{4T}{3\gamma} \left(s + \frac{2T^2\omega}{\pi^2} \cosh\left(\frac{\omega}{2T}\right) + (1 + e\chi_m) \frac{B^2}{T} - \frac{\Phi}{T} \right) \partial_\mu u^\mu \right] \quad (32)$$

The changing magnetic field induces the electric field, making the medium evolution more complex. Therefore, to reduce the complexity, we have considered a static magnetic field for our calculation, i.e., $\frac{dB}{d\tau} = 0$. In such a situation, Eq. (32) reduces to:

$$\frac{d\omega}{d\tau} = \frac{-\pi^2}{2G} \left[\left(s + 3dT^3 + \frac{2F}{\pi^2} \right) \frac{dT}{d\tau} \right]$$

$$+ \frac{4T}{3\gamma} \left(s + \frac{2T^2\omega}{\pi^2} \cosh\left(\frac{\omega}{2T}\right) + (1 + e\chi_m) \frac{B^2}{T} - \frac{\Phi}{T} \right) \partial_\mu u^\mu \quad (33)$$

The temperature evolution equation in the presence of vorticity and magnetic field coupling is given by,

$$\begin{aligned} \frac{dT}{d\tau} = & -\frac{T}{3\gamma} \left(1 + \frac{2\omega T^2}{s\pi^2} \cosh\left(\frac{\omega}{2T}\right) + \frac{\chi_m e B^2}{Ts} \right) \partial_\mu u^\mu \\ & + \frac{\Phi T^{-3}}{12a\gamma} \partial_\mu u^\mu \end{aligned} \quad (34)$$

We have used Eq. (29) to include the viscous effect in this case as well.

The following section presents the interplay among vorticity, viscosity, and temperature on their dissipation using the above-discussed formalism.

3 Results and discussion

This section explores the effect of rotation and viscous forces on the evolution of the QGP. Their individual and combined roles in the evolution of temperature are discussed. The vorticity, viscosity, and temperature evolution are governed respectively by the three coupled equations Eqs. (26), (29), and (27). The solution of these coupled differential equations is very sensitive to the initial conditions, i.e., T_0 , τ_0 , ω_0 and Φ_0 . We have considered the initial viscosity $\Phi_0 = \frac{1}{3\pi} \frac{s_0}{\tau_0}$ at $\tau = \tau_0$, where $s_0 = c + dT_0^3$ is the initial entropy density [50]. While the initial condition for vorticity is chosen in such a way that the speed of rotation does not violate the causality. Therefore, ω_0 is taken as $\omega \propto \frac{1}{\tau_0}$ to preserve the causality. Given these conditions, we have chosen three sets of initial conditions for T_0 , τ_0 , and ω_0 . Each set of initial conditions corresponds to a completely new evolving system. We have solved the coupled differential equation corresponding to T , ω , and Φ using these initial conditions. First, we illustrate how vorticity, viscosity, and temperature change with τ when there is no coupling between viscosity and vorticity. Next, we explore the scenario when viscosity contributes to the vorticity and their combined effect on temperature variation. Further, the direct contribution of vorticity in viscosity will be shown. It is to be noted that T_{Ideal} stands for the case when $\omega = 0$ and $\Phi = 0$ in Eq. (30). T_{SO} (T_{SO}^ω) stands for temperature obtained by solving the second-order hydrodynamic equations for $\omega = 0$ ($\omega \neq 0$). It is noteworthy to mention that for irrotational fluid ($\omega = 0$), the longitudinal boost invariant velocity profile is assumed, and the evolution is similar to a Bjorken-like flow. However, for the rotational fluid ($\omega \neq 0$) we consider the velocity profile mentioned in Eqs. (18) and (19).

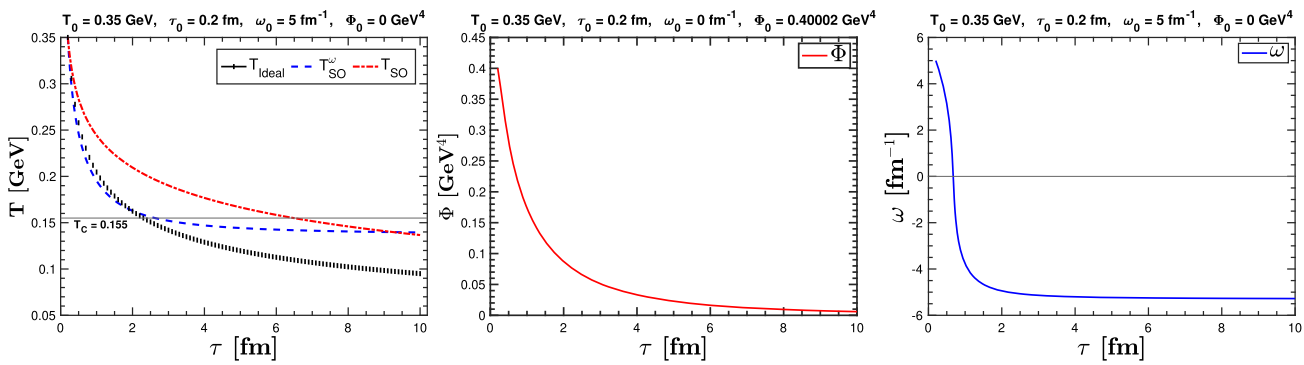


Fig. 1 Left to right: Temperature (T), viscous term (Φ) and vorticity (ω) are plotted, respectively, against time τ with the initial conditions: $T = 0.35 \text{ GeV}$, $\tau_0 = 0.2 \text{ fm}$, $\omega_0 = 0.1 \text{ fm}^{-1}$, $\Phi_0 = 0.40002 \text{ GeV}^4$. For $T_{\text{ideal}}; \omega = 0$ and $\Phi = 0$. For $T_{SO}; \omega = 0$ but $\Phi \neq 0$. For $T_{SO}^\omega; \omega \neq 0$ but $\Phi = 0$. In Φ plot, $\omega = 0$ and in ω plot, $\Phi = 0$

$T_{\text{ideal}}; \omega = 0$ and $\Phi = 0$. For $T_{SO}; \omega = 0$ but $\Phi \neq 0$. For $T_{SO}^\omega; \omega \neq 0$ but $\Phi = 0$. In Φ plot, $\omega = 0$ and in ω plot, $\Phi = 0$

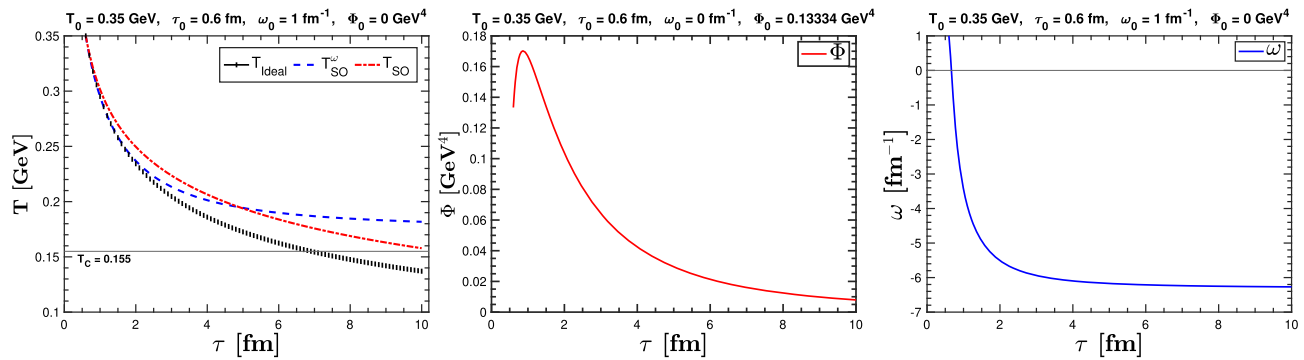


Fig. 2 Left to right: Temperature (T), viscous term (Φ) and vorticity (ω) are plotted, respectively, against time τ with the initial conditions: $T = 0.35 \text{ GeV}$, $\tau_0 = 0.6 \text{ fm}$, $\omega_0 = 1.0 \text{ fm}^{-1}$, $\Phi_0 = 0.13334 \text{ GeV}^4$. For $T_{\text{ideal}}; \omega = 0$ and $\Phi = 0$. For $T_{SO}; \omega = 0$ but $\Phi \neq 0$. For $T_{SO}^\omega; \omega \neq 0$ but $\Phi = 0$. In Φ plot, $\omega = 0$ and in ω plot, $\Phi = 0$

$T_{\text{ideal}}; \omega = 0$ and $\Phi = 0$. For $T_{SO}; \omega = 0$ but $\Phi \neq 0$. For $T_{SO}^\omega; \omega \neq 0$ but $\Phi = 0$. In Φ plot, $\omega = 0$ and in ω plot, $\Phi = 0$

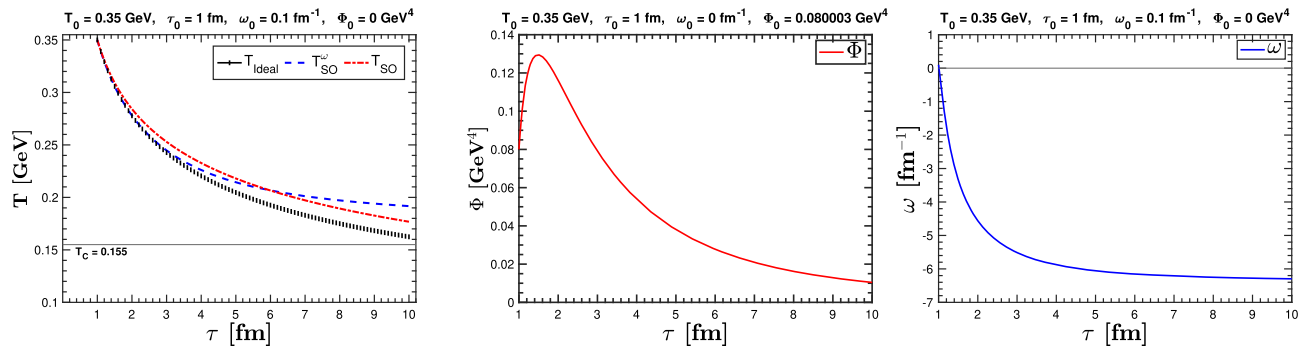


Fig. 3 Left to right: Temperature (T), viscous term (Φ) and vorticity (ω) are plotted, respectively, against time τ with the initial conditions: $T = 0.35 \text{ GeV}$, $\tau_0 = 1 \text{ fm}$, $\omega_0 = 0.1 \text{ fm}^{-1}$, $\Phi_0 = 0.080003 \text{ GeV}^4$. For $T_{\text{ideal}}; \omega = 0$ and $\Phi = 0$. For $T_{SO}; \omega = 0$ but $\Phi \neq 0$. For $T_{SO}^\omega; \omega \neq 0$ but $\Phi = 0$. In Φ plot, $\omega = 0$ and in ω plot, $\Phi = 0$

$T_{\text{ideal}}; \omega = 0$ and $\Phi = 0$. For $T_{SO}; \omega = 0$ but $\Phi \neq 0$. For $T_{SO}^\omega; \omega \neq 0$ but $\Phi = 0$. In Φ plot, $\omega = 0$ and in ω plot, $\Phi = 0$

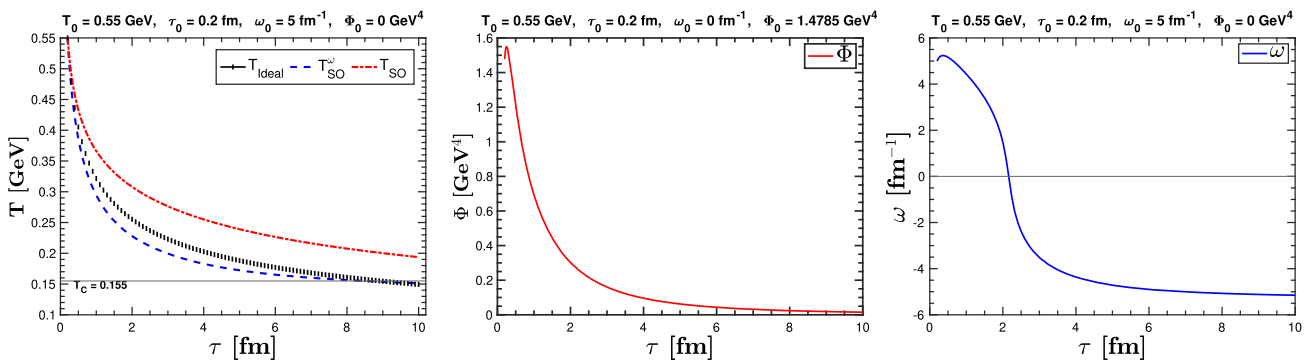


Fig. 4 Left to right: Temperature (T), viscous term (Φ) and vorticity (ω) are plotted, respectively, against time τ with the initial conditions: $T = 0.55 \text{ GeV}$, $\tau_0 = 0.2 \text{ fm}$, $\omega_0 = 5 \text{ fm}^{-1}$, $\Phi_0 = 1.4785 \text{ GeV}^4$. For

$T_{\text{ideal}}; \omega = 0$ and $\Phi = 0$. For T_{SO} ; $\omega = 0$ but $\Phi \neq 0$. For T_{SO}^ω ; $\omega \neq 0$ but $\Phi = 0$. In Φ plot, $\omega = 0$ and in ω plot, $\Phi = 0$

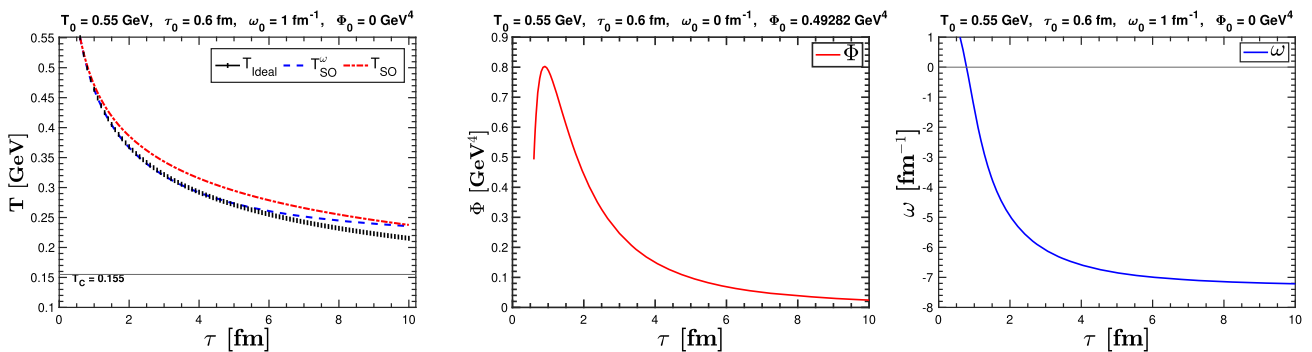


Fig. 5 Left to right: Temperature (T), viscous term (Φ) and vorticity (ω) are plotted, respectively, against time τ with the initial conditions: $T = 0.55 \text{ GeV}$, $\tau_0 = 0.6 \text{ fm}$, $\omega_0 = 1 \text{ fm}^{-1}$, $\Phi_0 = 0.49282 \text{ GeV}^4$. For

$T_{\text{ideal}}; \omega = 0$ and $\Phi = 0$. For T_{SO} ; $\omega = 0$ but $\Phi \neq 0$. For T_{SO}^ω ; $\omega \neq 0$ but $\Phi = 0$. In Φ plot, $\omega = 0$ and in ω plot, $\Phi = 0$

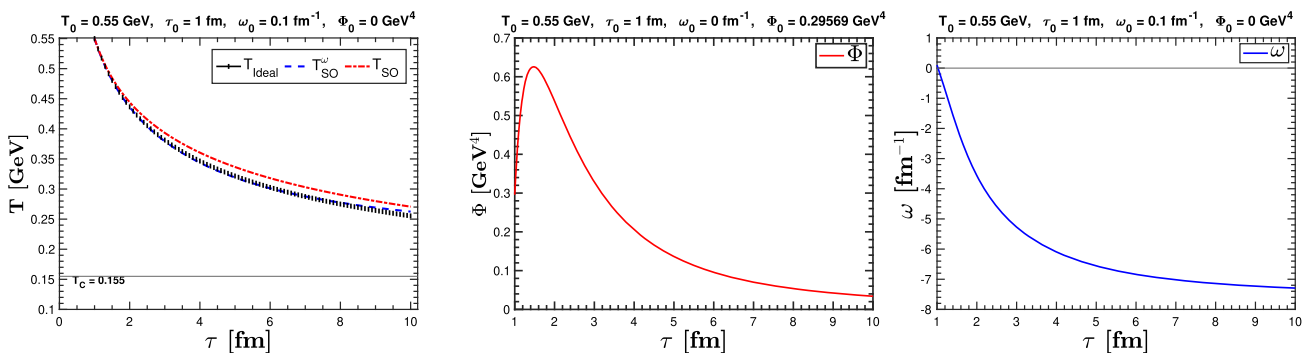


Fig. 6 Left to right: Temperature (T), viscous term (Φ) and vorticity (ω) are plotted, respectively, against time τ with the initial conditions: $T = 0.55 \text{ GeV}$, $\tau_0 = 1 \text{ fm}$, $\omega_0 = 0.1 \text{ fm}^{-1}$, $\Phi_0 = 0.29569 \text{ GeV}^4$. For

$T_{\text{ideal}}; \omega = 0$ and $\Phi = 0$. For T_{SO} ; $\omega = 0$ but $\Phi \neq 0$. For T_{SO}^ω ; $\omega \neq 0$ but $\Phi = 0$. In Φ plot, $\omega = 0$ and in ω plot, $\Phi = 0$

Case I: No coupling between Φ and ω

The individual effect of ω and Φ on medium cooling is explored in this section. The corresponding differential equations for the cooling are:

$$\frac{dT}{d\tau} = -\frac{T}{3\gamma} \left[1 + \frac{2\omega T^2}{s\pi^2} \cosh\left(\frac{\omega}{2T}\right) \right] \partial_\mu u^\mu$$

$$\frac{dT}{d\tau} = \frac{1}{\gamma} \left[-\frac{T}{3} + \frac{\Phi T^{-3}}{12a} \right] \partial_\mu u^\mu$$

The solutions of these two equations are T_{SO}^ω and T_{SO} respectively.

In Fig. 1, rapid cooling is observed for ideal fluid in the absence of any dissipation. In presence of viscosity additional heat production reduces the cooling. Similar to viscosity, vorticity too affects the cooling. Vortical motion present in the QGP medium imposes a constraint on the medium cooling. During the first moments of evolution, the rotation speed is almost equal to the medium evolution rate; due to this, it does not affect the cooling rate much. Therefore, as shown in Fig. 1, initially upto $\tau \sim 2$ fm the cooling rate of $T_{SO}^\omega \approx T_{\text{Ideal}}$. Afterward, the system tries to hold back the evolution process when the rotation speed becomes smaller than the fluid velocity. The ω diffusion and Φ dissipation with time is plotted in Fig. 1, initially ω changes with a high rate, but at a later stage, it becomes almost constant in the absence of any other external force while Φ approaches zero at large τ . The negative value of ω in the plot depicts the change in the direction of the rotation. This change in the rotation happens due to the initial fast expansion of the medium and the restriction imposed on it by the rotational motion of the fluid. This means medium evolution induces the rotation opposite to the initial vorticity. As time increases, vorticity also grows/diffuses in the opposite direction and gets saturated when medium evolution becomes static. Results displayed in Fig. 1 also suggest that cooling becomes almost independent of the vorticity if fluid is rotating close to the speed of light and, therefore, the cooling rate at $\omega_0 = 5 \text{ fm}^{-1}$ becomes almost the same as the ideal one, i.e., $T_{SO}^\omega \approx T_{\text{Ideal}}$.

Figures 2 and 3 depicts the cooling rate change with changing initial conditions. The variation of T_{SO}^ω cooling shown in Figs. 2 and 3 is the implication of low speed of the rotation along with the change in other initial conditions as compared to Fig. 1. Depending on the speed of the medium rotation, the ω evolution is shown in Figs. 2 and 3. The large value of τ_0 reduces the Φ_0 , which leads to a faster cooling for T_{SO} . When the temperature cooling is faster than the Φ dissipation rate, it induces the medium viscosity, which causes a smooth rise in Φ as seen in the viscous evolution displayed in Figs. 2 and 3.

Now we take $T_0 = 0.550 \text{ GeV}$ and keep the same initial conditions for Φ_0 and ω_0 as earlier and evaluate T , Φ , and

ω to check the sensitivity of the results on the value of initial temperature. The results in such cases are shown in Fig. 4, 5 and 6. The results show that the high initial vorticity effect almost vanishes at a relatively high initial temperature. As a result, the cooling for non-viscous rotating fluid behaves like ideal fluid. The dissipation of ω with proper time plotted in Fig. 4, shows that temperature and vorticity coupling dominate when both are very large at the initial stage ($T_0 = 0.550 \text{ GeV}$ and $\omega_0 = 5.0 \text{ fm}^{-1}$). The short thermalization time and large initial temperature provide a large initial viscosity, reducing the cooling for T_{SO} respective to Fig. 1. Figure 4 depicts that the vorticity diffusion rate is slow until a certain time; thereafter, vorticity increases in the opposite direction and gets saturated with time. Figures 5 and 6 follow similar trend as Figs. 3 and 4 with higher initial temperature.

Case-II: Φ coupling with ω

In this case, we have considered both non-zero viscosity and vorticity in determining the cooling rate as given in Eq. (27). $T_{SO-\Phi}^\omega$ in the figures represents the cooling rate corresponding to Eq. (27) and ω^Φ stands for the vorticity obtained by solving Eq. (26). Here we see how viscosity in a rotating fluid modifies the cooling rate and vorticity evolution (ω^Φ).

In Fig. 7, the combination of vorticity and viscosity is shown for large initial vorticity and a small thermalization time. $T_{SO-\Phi}^\omega$ cools down slightly faster than T_{SO} due to the opposition of viscosity to changes in vorticity direction. Positive initial vorticity results in faster cooling, almost following the ideal rate. However, the presence of viscosity in the rotating fluid slows down $T_{SO-\Phi}^\omega$ cooling compared to T_{Ideal} . The impact of viscosity on vorticity change can be observed in the variation of ω^Φ as shown in Fig. 7. The Φ evolution shown in Fig. 7 follows similar pattern as the corresponding result shown in Fig. 1. In Fig. 8, the combined dynamics of ω and Φ are shown for an initial vorticity value of $\omega_0 = 1.0 \text{ fm}^{-1}$ and a thermalization time of $\tau_0 = 0.6 \text{ fm}$. A relatively smaller initial viscosity value is insufficient to resist rapid changes in vorticity. Smaller vorticities easily adapt to the changes imposed by the evolving medium. Negative vorticity slows down the cooling rate, resulting in $T_{SO-\Phi}^\omega$ cooling at a slower rate than T_{SO} . In Fig. 8, the coupling between Φ and ω leads to the activation of a saturation point in the diffusion rate of ω^Φ . The Φ evolution plot in Fig. 8 follows a similar pattern to its corresponding plot in Fig. 2. Figure 9 follows similar explanation as Fig. 8, with cooling becoming even slower for $T_{SO-\Phi}^\omega$ due to a very small initial vorticity and a large thermalization time.

What happens if, along with initial vorticity, the initial temperature is large and the thermalization time is short? The answer to this question is given in Fig. 10; it implies that at low τ_0 and high T_0 , the initial viscosity is very high. As

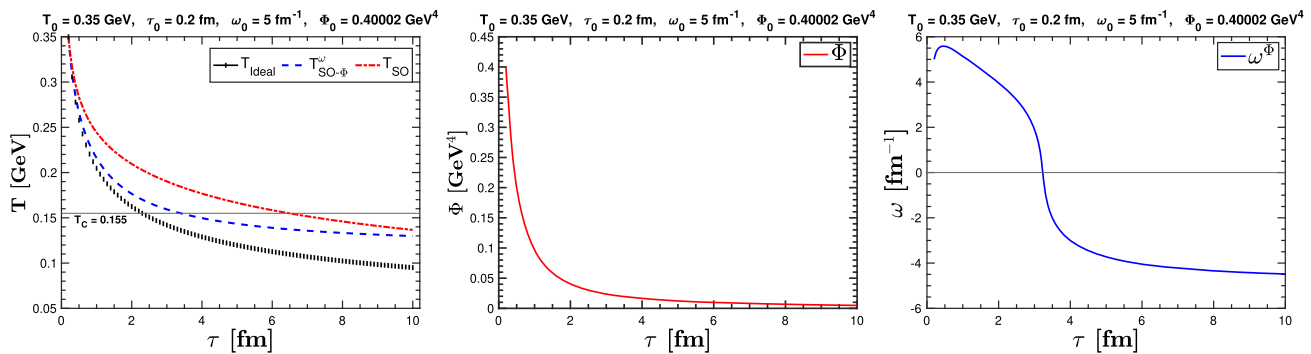


Fig. 7 Left to right: Temperature (T), viscous term (Φ) and vorticity (ω) are plotted, respectively, against time τ with the initial conditions: $T = 0.35 \text{ GeV}$, $\tau_0 = 0.2 \text{ fm}$, $\omega_0 = 5.0 \text{ fm}^{-1}$, $\Phi_0 = 0.40002 \text{ GeV}^4$

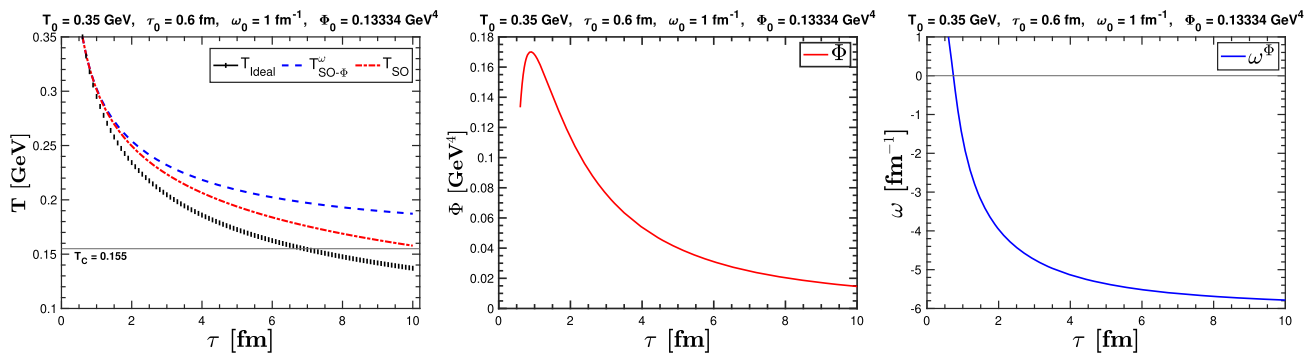


Fig. 8 Left to right: Temperature (T), viscous term (Φ) and vorticity (ω) are plotted, respectively, against time τ with the initial conditions: $T = 0.35 \text{ GeV}$, $\tau_0 = 0.6 \text{ fm}$, $\omega_0 = 1.0 \text{ fm}^{-1}$, $\Phi_0 = 0.13334 \text{ GeV}^4$

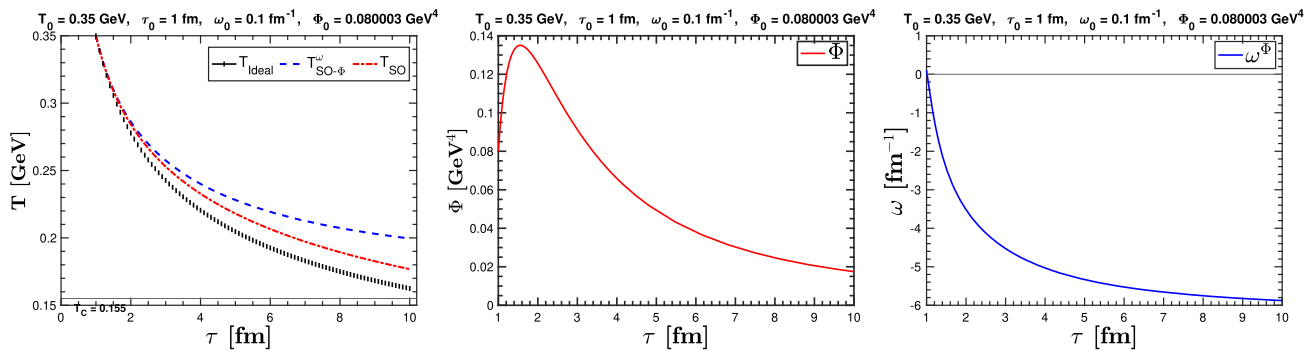


Fig. 9 Left to right: Temperature (T), viscous term (Φ) and vorticity (ω) are plotted, respectively, against time τ with the initial conditions: $T = 0.35 \text{ GeV}$, $\tau_0 = 1.0 \text{ fm}$, $\omega_0 = 0.1 \text{ fm}^{-1}$, $\Phi_0 = 0.080003 \text{ GeV}^4$

discussed earlier, due to viscosity coupling with vorticity and their large initial values make cooling faster; if the medium temperature is also high, cooling becomes even faster. As all these mentioned conditions are fulfilled in Fig. 10, the cooling for $T_{SO-\Phi}^\omega$ becomes very fast that medium gets exhausted much before T_{Ideal} . The combined effect of large viscosity and the high temperature does not let the evolving medium change the direction of the vorticity, as shown in the $\omega - \tau$ plot of Fig. 10, where ω is always positive and vanishes when $T \rightarrow 0$. Due to this coupling, Φ gets dissipated earlier.

Figure 11 depicts that decrease of ω_0 and increase of τ_0 , makes the variation of $T_{SO-\Phi}^\omega$ and T_{Ideal} similar. However, $T_{SO-\Phi}^\omega$ remains faster in the region, which represents faster cooling than T_{SO} . While ω_0 and Φ_0 are small, the high T_0 and Φ_0 together support vorticity to sustain its initial direction till temperature and viscosity become inefficient to restrict the change. The change in the cooling rate corresponding to very small vorticity and very large thermalization time and temperature is depicted in Fig. 12. In this scenario, the variation of $T_{SO-\Phi}^\omega$ and T_{SO} turns out to be similar. Here the impact of viscosity is minimal on vorticity. The high initial

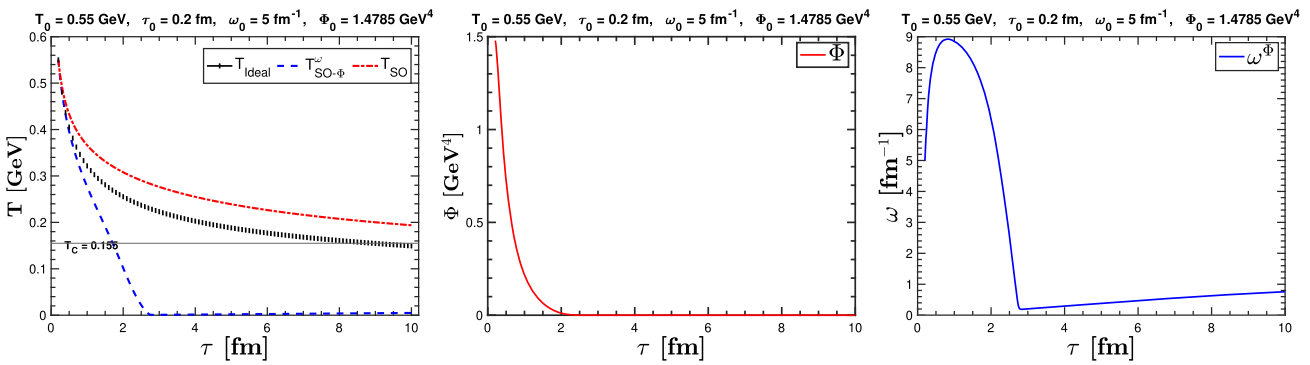


Fig. 10 Left to right: Temperature (T), viscous term (Φ) and vorticity (ω) are plotted, respectively, against time τ with the initial conditions: $T = 0.55 \text{ GeV}$, $\tau_0 = 0.2 \text{ fm}$, $\omega_0 = 5.0 \text{ fm}^{-1}$, $\Phi_0 = 1.4785 \text{ GeV}^4$

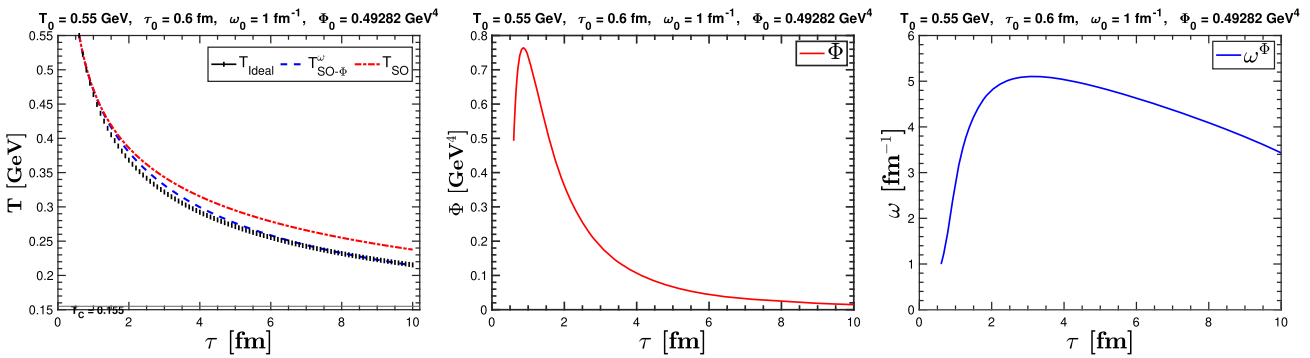


Fig. 11 Left to right: Temperature (T), viscous term (Φ) and vorticity (ω) are plotted, respectively, against time τ with the initial conditions: $T = 0.55 \text{ GeV}$, $\tau_0 = 0.6 \text{ fm}$, $\omega_0 = 1.0 \text{ fm}^{-1}$, $\Phi_0 = 0.49282 \text{ GeV}^4$

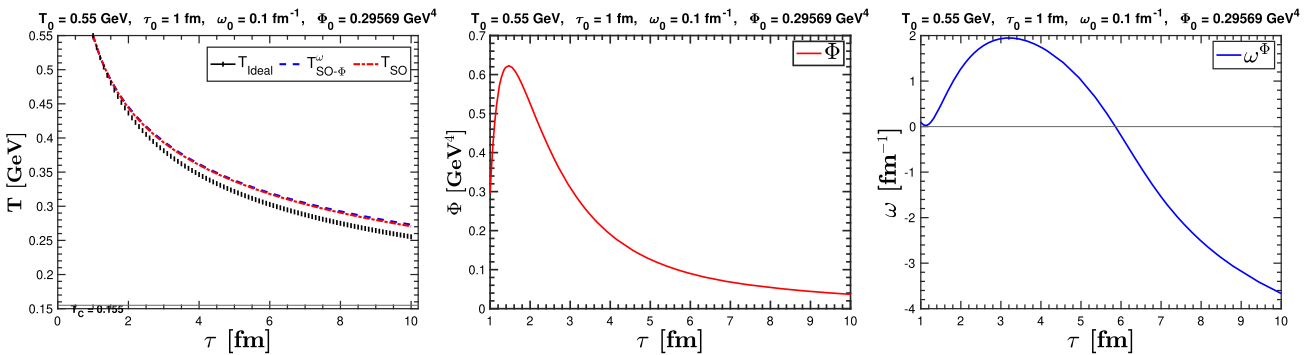


Fig. 12 Left to right: Temperature (T), viscous term (Φ) and vorticity (ω) are plotted, respectively, against time τ with the initial conditions: $T = 0.55 \text{ GeV}$, $\tau_0 = 1.0 \text{ fm}$, $\omega_0 = 0.1 \text{ fm}^{-1}$, $\Phi_0 = 0.29569 \text{ GeV}^4$

temperature is a dominating factor in this case. Therefore a small rise in ω for a short duration is observed in Fig. 12. Later it diffuses in the opposite direction; as a result, the cooling rate corresponding to $T_{SO-\Phi}^\omega \sim T_{SO}$ and it becomes slightly slower than T_{SO} around $\tau > 7.0 \text{ fm}$.

Case-III: Direct coupling of ω with Φ

In earlier cases, ω was not directly contributing in the viscous term as the last term of Eq. (29) was taken as $\frac{\omega\Phi}{\gamma T\tau} = 0$. Similar to the previous case, viscosity induces a rotational

motion in the fluid. In the same way, rotating fluid induces an additional viscosity in the medium due to the velocity gradient between rotating fluid cells. This coupling between ω and Φ plays a complementary role in the medium evolution. The temperature variation of $\omega - \Phi$ coupling is presented by $T_{SO}^{\omega\Phi}$ which corresponds to the solution of the coupled rate equations; Eqs. (26), (27) and (29). The rate of change in Φ due to its direct coupling with ω is shown by Φ^ω .

The results for a fixed initial temperature, $T_0 = 0.350 \text{ GeV}$, are presented in Fig. 13, 14 and 15. In Fig. 13, it can be observed that a higher value of ω_0 causes Φ to decrease to

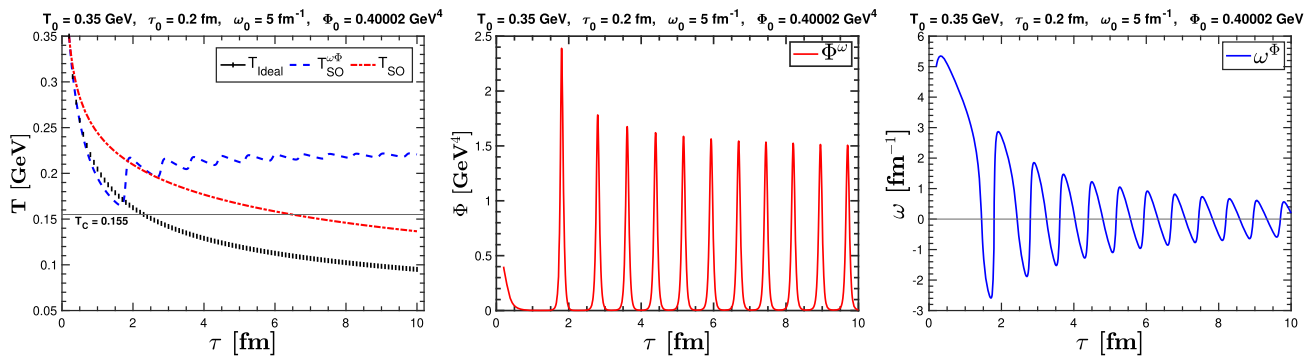


Fig. 13 Left to right: Temperature (T), viscous term (Φ) and vorticity (ω) are plotted, respectively, against time τ with the initial conditions: $T = 0.35 \text{ GeV}$, $\tau_0 = 0.2 \text{ fm}$, $\omega_0 = 5.0 \text{ fm}^{-1}$, $\Phi_0 = 0.40002 \text{ GeV}^4$

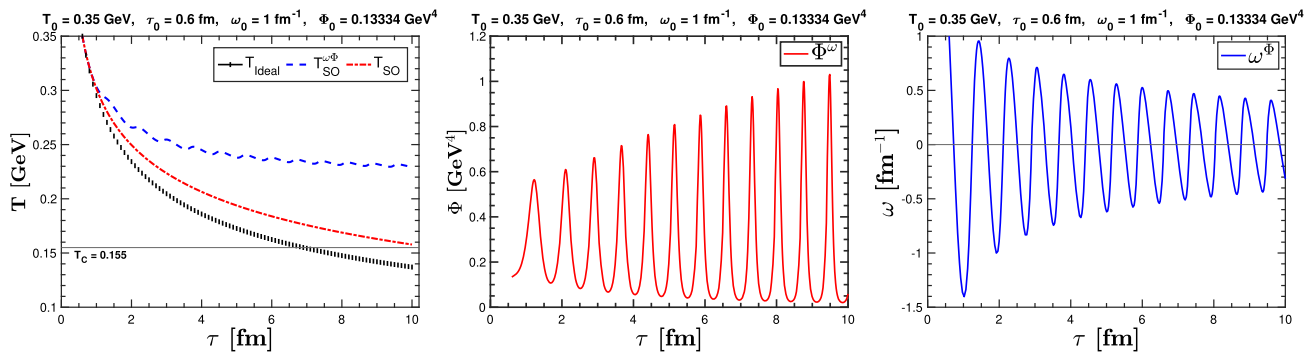


Fig. 14 Left to right: Temperature (T), viscous term (Φ) and vorticity (ω) are plotted, respectively, against time τ with the initial conditions: $T = 0.35 \text{ GeV}$, $\tau_0 = 0.6 \text{ fm}$, $\omega_0 = 1.0 \text{ fm}^{-1}$, $\Phi_0 = 0.13334 \text{ GeV}^4$

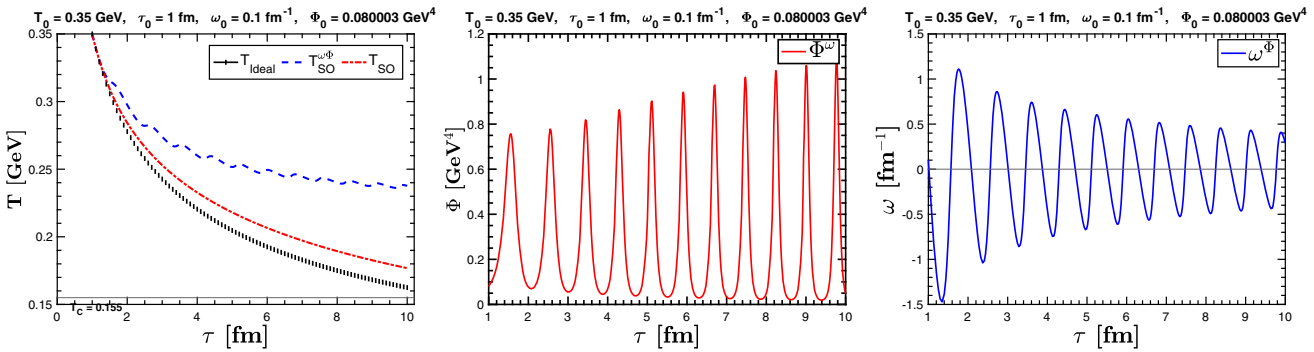


Fig. 15 Left to right: Temperature (T), viscous term (Φ) and vorticity (ω) are plotted, respectively, against time τ with the initial conditions: $T = 0.35 \text{ GeV}$, $\tau_0 = 1.0 \text{ fm}$, $\omega_0 = 0.1 \text{ fm}^{-1}$, $\Phi_0 = 0.080003 \text{ GeV}^4$

zero, resulting in $T_{SO}^{\omega\Phi}$ cooling being equivalent to T_{ideal} . Conversely, a large negative value of ω leads to a sharp increase in Φ , causing an abrupt change in $T_{SO}^{\omega\Phi}$ around $\tau = 2 \text{ fm}$. This sudden rise in Φ changes the direction of ω . On the whole, $+\omega$ decreases the Φ and $-\omega$ increases it. Similarly, Non-zero Φ generates the vorticity in the opposite direction of the existing vorticity. This cyclic process produces oscillations in ω and Φ cooling, as observed in Fig. 13. Consequently, $T_{SO}^{\omega\Phi}$ cooling becomes very slow, resembling a damped step function over time. For diluted initial conditions, as depicted in Fig. 14, $T_{SO}^{\omega\Phi}$ does not exhibit any abrupt changes in cool-

ing. However, the cooling process becomes very slow in this case due to the increasing oscillation of Φ over time, caused by the relatively small initial vorticity ($\omega_0 = 1.0 \text{ fm}^{-1}$) and viscosity ($\Phi_0 = 0.13334 \text{ GeV}^4$). The low viscosity accelerates the evolution, generating significant vorticity in the opposite direction, which increases $-\omega$. Due to the small ω_0 , Φ is not completely dissipated and instead adds up to the viscosity induced by $-\omega$. Consequently, the peak of Φ increases with each oscillation, establishing a self-sustaining system that does not dissipate over time. Figure 15 follows

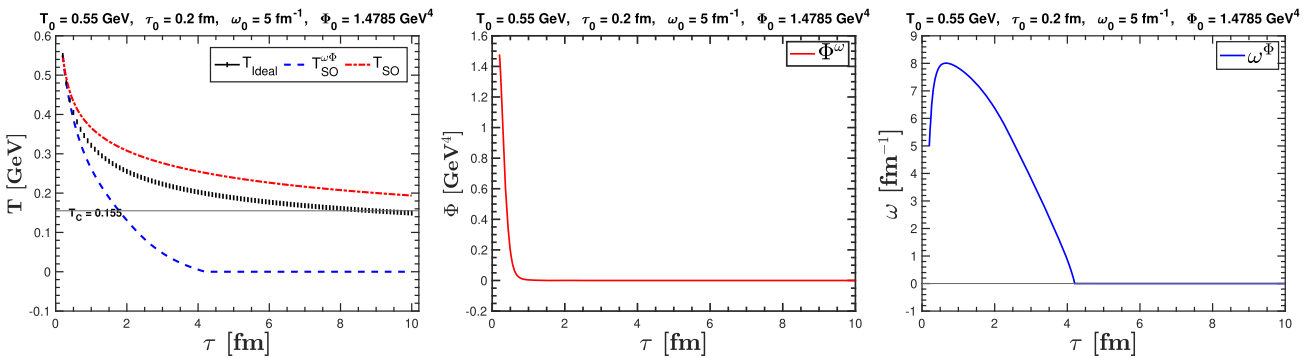


Fig. 16 Left to right: Temperature (T), viscous term (Φ) and vorticity (ω) are plotted, respectively, against time τ with the initial conditions: $T = 0.55 \text{ GeV}$, $\tau_0 = 0.2 \text{ fm}$, $\omega_0 = 5.0 \text{ fm}^{-1}$, $\Phi = 1.4785 \text{ GeV}^4$

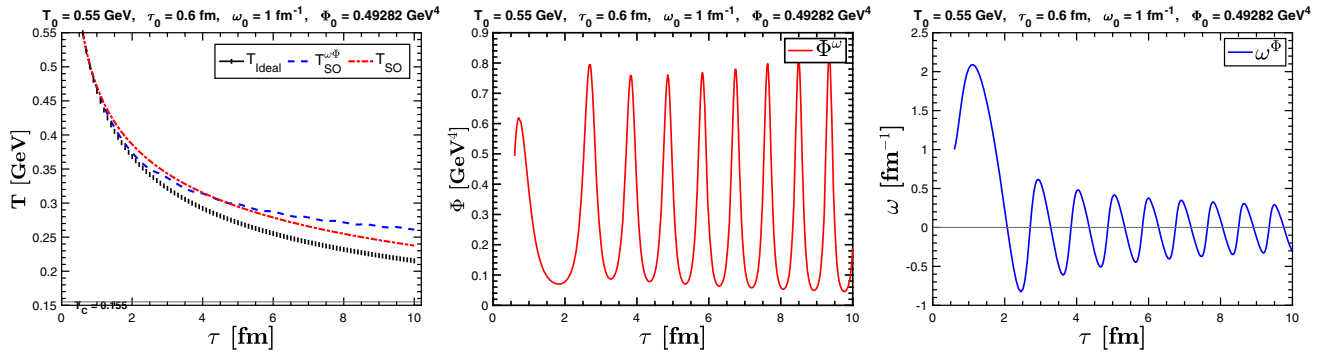


Fig. 17 Left to right: Temperature (T), viscous term (Φ) and vorticity (ω) are plotted, respectively, against time τ with the initial conditions: $T = 0.55 \text{ GeV}$, $\tau_0 = 0.6 \text{ fm}$, $\omega_0 = 1.0 \text{ fm}^{-1}$, $\Phi = 0.49282 \text{ GeV}^4$

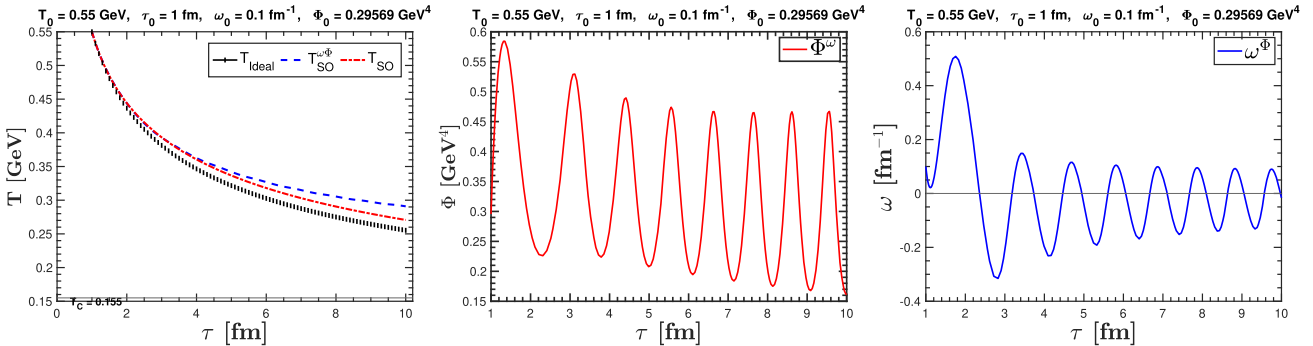


Fig. 18 Left to right: Temperature (T), viscous term (Φ) and vorticity (ω) are plotted, respectively, against time τ with the initial conditions: $T = 0.55 \text{ GeV}$, $\tau_0 = 1.0 \text{ fm}$, $\omega_0 = 0.1 \text{ fm}^{-1}$, $\Phi = 0.29569 \text{ GeV}^4$

the same trend as Fig. 14, with the magnitude differences reflecting the use of different initial conditions.

We adopt the same initial conditions for τ_0 and ω_0 at a higher initial temperature $T_0 = 0.550 \text{ GeV}$. Figure 16 demonstrates that at the high initial temperature, vorticity and viscosity coupling ($\omega - \Phi$) enable fluid rotation in one direction, leading to a sudden drop in Φ . Consequently, all these systems cool down at a faster rate than the ideal case, and vorticity also diminishes over time. This behavior is reflected in $T_{SO}^{\omega\Phi}$ as shown in Fig. 16. Furthermore, when Φ_0 and ω_0 are small, the $\omega - \Phi$ coupling induces oscillations in vorticity

and Φ over time. At high initial temperatures, the damping of ω and Φ is more pronounced compared to the results displayed in Fig. 14, resulting in smaller oscillation amplitudes, as depicted in Fig. 17. Consequently, $T_{SO}^{\omega\Phi}$ dissipates faster in Fig. 17 compared to the case shown in Fig. 14. However, $T_{SO}^{\omega\Phi}$ cooling remains slow and oscillatory compared to its cooling rate depicted in Fig. 16. The slight oscillation in $T_{SO}^{\omega\Phi}$ in Fig. 17 arises from finite ω and Φ oscillations. If we further decrease ω_0 at high τ_0 , the oscillation in $T_{SO}^{\omega\Phi}$ disappears. In this scenario, we observe an opposite damped shift in ω and Φ oscillations, as shown in Fig. 18. Here, the positive ω phase

increases slowly, while the negative ω phase decreases at a faster rate, resulting in damped oscillations in Φ . Overall, in this case, $\omega - \Phi$ compensate each other in a way that $T_{SO}^{\omega\Phi}$ exhibits continuous and slow cooling compared to T_{SO} , as depicted in Fig. 18.

Case IV: Change in the medium evolution due to the static magnetic field (B)

Considering an external static magnetic field (B) along with vorticity and viscosity, changes the hydrodynamical evolution of the medium. Here are a few scenarios for combining the magnetic field with non-viscous, viscous, and vorticity. We have considered the impact of the static magnetic field ($B \neq 0$) in the following cases:

- At, $\omega = 0, \Phi = 0$; we get the temperature evolution for an ideal case in the presence of the static magnetic field as,

$$\frac{dT}{d\tau} = -\frac{T}{3\gamma} \left(1 + \frac{\chi_m e B^2}{T_s} \right) \partial_\mu u^\mu$$

We call the solution of this equation as $T_{Ideal+B}$. Here χ_m is magnetic susceptibility, in our calculation we have taken $\chi_m = 0.03$ [49] and $eB = 10m_\pi^2$. The net electric charge is considered taking the sum over the electric charges of u, d , and s quarks to obtain the magnetic field; $eB = \sum_f |q_f|B$.

- Now we consider that $\omega = 0$, but medium has finite viscosity, $\Phi \neq 0$.

$$\frac{dT}{d\tau} = \left[-\frac{T}{3\gamma} \left(1 + \frac{\chi_m e B^2}{T_s} \right) + \frac{\Phi T^{-3}}{12a\gamma} \right] \partial_\mu u^\mu$$

The solution of this equation is denoted as T_{SO+B}

- Next, we assume that medium is viscous and has vorticity as well, s.t. $\omega \neq 0, \Phi \neq 0$. However, in this case, Φ does not arise due to vorticity, while vorticity gets induced due to viscosity. So the cooling respective to the mentioned condition is defined in Eq. (34) is represented here as; $T_{SO+\Phi}^{\omega+B}$, and corresponding vorticity and viscosity dissipation with time are depicted by $\omega^{B\Phi}$ and Φ^B , respectively.
- Further, we consider the case when vorticity and viscosity play a complementary relation, i.e., $\omega(\Phi)$ and $\Phi(\omega)$. The change of viscosity and vorticity dissipation under $\omega - \Phi$ coupling in the presence of magnetic field (B) is denoted as $T_{SO}^{\omega\Phi+B}$, $\Phi^{\omega\Phi+B}$ and $\omega^{\omega\Phi+B}$, respectively.

Figure 19 shows that inclusion of static magnetic field along with vorticity and viscosity does not let the medium cool down. As seen in the T vs. τ plot, the solid blue line

initially decreases and slowly increases with time. While the magnetic field for the ideal and viscous case slightly increases the cooling. It can be interpreted in this way that the magnetic field separates the +ve and -ve charge particles in opposite directions to create charge polarization in the medium. This charge polarization gives a boost to the cooling. Therefore inclusion of a magnetic field makes cooling faster in the absence of vorticity. The vorticity or rotation in the medium disturbs the charge polarization while the magnetic field works to retain it. In this process, the magnetic field drastically increases the vorticity in the opposite direction, as depicted in the ω vs. τ plot in Fig. 19. Because of this, the viscous term Φ also gets altered, and its dissipation rate gets reduced, as shown by the dashed black line in Φ vs. τ plot in Fig. 19.

Figure 20 shows the changes brought in the medium evolution due to the $\omega - \Phi$ coupling in the presence of the static magnetic field. The oscillations in dissipation rates follow a similar explanation as the previous results of $\omega - \Phi$ coupling where $B = 0$. Here, the non-zero static magnetic field enhances the amplitude of the damped oscillatory solutions for ω , which can be witnessed in Fig. 20. The magnetic field along with $\omega - \Phi$ coupling also largely enhances the fluctuation in viscosity, $\Phi^{\omega\Phi+B}$, dissipation rate as compared with $B = 0$ case, i.e. $\Phi^{\omega\Phi}$. This $\omega - \Phi$ coupling, along with B , produces an additional heat which raises the temperature $T > T_0$ when vorticity is maximum ($\omega \approx -5.0 \text{ fm}^{-1}$) as depicted in Fig. 20. It also shows that the cooling of the medium becomes stagnant if $\omega - \Phi$ coupling occurs in the presence of the static magnetic field. Figures 19 and 20 suggest that a non-zero static magnetic field induces a shift in the temperature (T), viscosity (Φ) and vorticity (ω) dissipation rate if the medium has finite initial vorticity.

4 Summary

Within the ambit of second-order causal dissipative hydrodynamics, we have investigated the impact of vorticity on the evolution of viscous QGP and compared the results with the evolution of an ideal QGP. We have found that the medium evolution is very sensitive to the initial temperature (T), the viscous term (Φ) as well as on vorticity (ω). These initial conditions significantly modify the medium evolution and QGP lifetime. Evolution becomes more complex with the coupling of vorticity and viscosity. Such a complementary relation between ω and Φ generates oscillations or fluctuations in the medium dissipation. In addition, the inclusion of a static magnetic field vastly reduces the cooling rate. We have adopted a simplified approach to a complex system with some conjectured velocity profiles to describe the medium created in ultra-relativistic collisions. However, considering a coupled system of vorticity, viscosity, and time-dependent

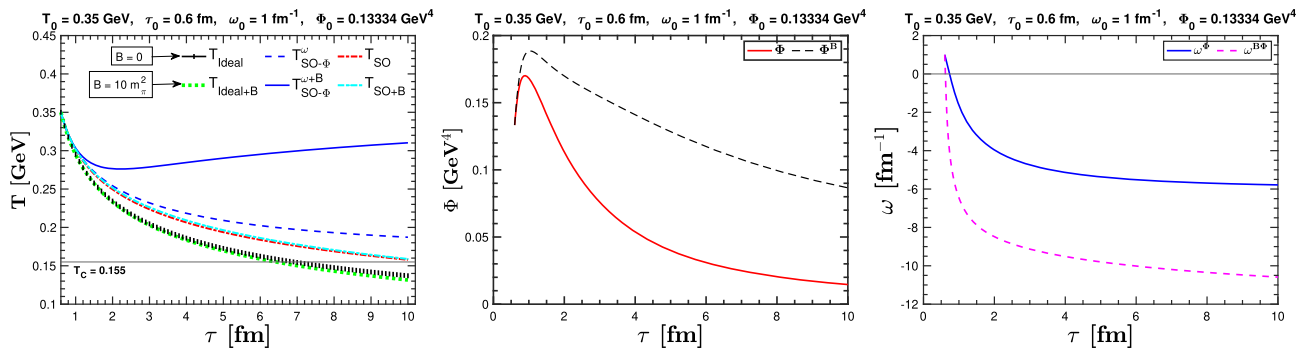


Fig. 19 Left to right: Temperature (T), viscous term (Φ) and vorticity (ω) are plotted, respectively, against time τ with the initial conditions: $T = 0.35 \text{ GeV}$, $\tau_0 = 0.6 \text{ fm}$, $\omega_0 = 1.0 \text{ fm}^{-1}$, $\Phi_0 = 0.13334 \text{ GeV}^4$

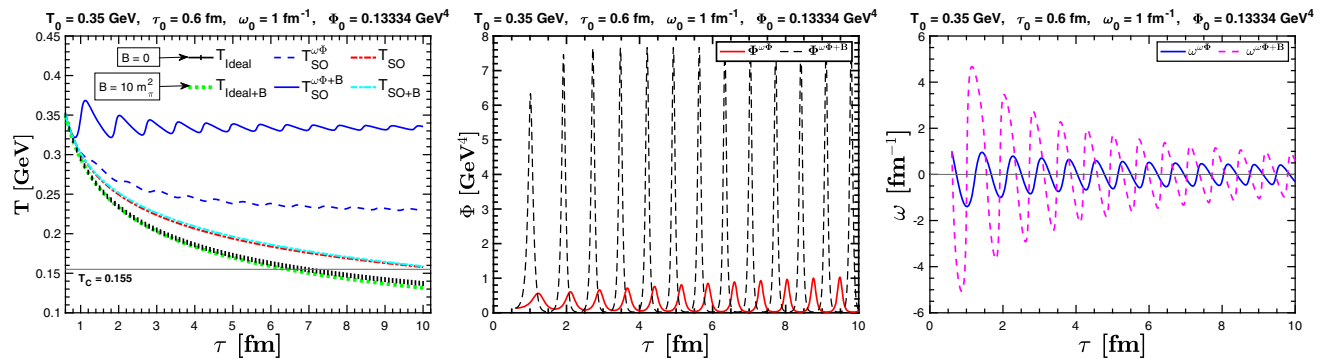


Fig. 20 Left to right: Temperature (T), viscous term (Φ) and vorticity (ω) are plotted, respectively, against time τ with the initial conditions: $T = 0.35 \text{ GeV}$, $\tau_0 = 0.6 \text{ fm}$, $\omega_0 = 1.0 \text{ fm}^{-1}$, $\Phi_0 = 0.13334 \text{ GeV}^4$

magnetic field along with its associated electric field in a (3+1)D hydrodynamics is a more realistic picture of QGP medium evolution. The evolution of QGP incorporates the interplay between various physical phenomena, which makes its cooling very complex.

Acknowledgements Raghunath Sahoo and Captain R. Singh acknowledge the financial support under DAE-BRNS, the Government of India, Project No. 58/14/29/2019-BRNS. Bhagyarthi Sahoo acknowledges the Council of Scientific and Industrial Research, Govt. of India, for financial support. The authors acknowledge the Tier-3 computing facility in the experimental high-energy physics laboratory of IIT Indore, supported by the ALICE project.

Data Availability Statement This manuscript has no associated data or the data will not be deposited. [Authors' comment: This is a theoretical paper. The associated data could be made available with a reasonable request to the authors.]

Open Access This article is licensed under a Creative Commons Attribution 4.0 International License, which permits use, sharing, adaptation, distribution and reproduction in any medium or format, as long as you give appropriate credit to the original author(s) and the source, provide a link to the Creative Commons licence, and indicate if changes were made. The images or other third party material in this article are included in the article's Creative Commons licence, unless indicated otherwise in a credit line to the material. If material is not included in the article's Creative Commons licence and your intended

use is not permitted by statutory regulation or exceeds the permitted use, you will need to obtain permission directly from the copyright holder. To view a copy of this licence, visit <http://creativecommons.org/licenses/by/4.0/>.

Funded by SCOAP³. SCOAP³ supports the goals of the International Year of Basic Sciences for Sustainable Development.

Appendix A: Calculation of $u^\mu \partial_\mu$

The convective derivative $u^\mu \partial_\mu$ is obtained as;

$$u^\mu \partial_\mu = u^0 \partial_0 + u^x \partial_x + u^y \partial_y + u^z \partial_z \quad (\text{A1})$$

Using the four velocity $u^\mu = \gamma(1, v_x, 0, v_z)$, we have

$$u^\mu \partial_\mu = \gamma \left(\frac{\partial}{\partial t} + v_x \frac{\partial}{\partial x} + v_z \frac{\partial}{\partial z} \right) \quad (\text{A2})$$

In the present scenario, we approximate a constant temperature and viscosity along the x and z directions. In mid-rapidity region (in the limit $\eta \rightarrow 0$) the above expression becomes,

$$u^\mu \partial_\mu = \gamma \frac{\partial}{\partial \tau} \quad (\text{A3})$$

Appendix B: Calculation of $\partial_\mu u^\mu$

The expansion rate $\partial_\mu u^\mu$ explore the velocity gradient, as given by;

$$\partial_\mu u^\mu = \partial_0 u^0 + \partial_x u^x + \partial_y u^y + \partial_z u^z \quad (\text{B1})$$

With the help of four velocity u^μ , we get;

$$\partial_\mu u^\mu = \left(\frac{\partial \gamma}{\partial t} + \frac{\partial(\gamma v_x)}{\partial x} + \frac{\partial(\gamma v_z)}{\partial z} \right) \quad (\text{B2})$$

Solving the above expression by using the velocity profile mentioned in Eqs. (18) and (19), we obtain;

$$\partial_\mu u^\mu = \left[\frac{\gamma}{\tau} + \frac{\gamma^3}{2} \left(\frac{\omega^2 x^2}{2\tau} - \frac{\omega x z}{\tau^2} \right) \right] \quad (\text{B3})$$

In the limit $\eta \rightarrow 0$,

$$\partial_\mu u^\mu = \frac{\gamma}{\tau} \left(1 + \frac{\gamma^2 \omega^2 x^2}{4} \right) \quad (\text{B4})$$

For irrotational fluid ($\omega = 0$) the divergence of velocity profile $\partial_\mu u^\mu$ is equal to $\frac{\gamma}{\tau}$.

Appendix C: Calculation of $\nabla^{<0} u^0 > - \nabla^{<z} u^z >$

We know,

$$\nabla^{<\mu} u^{\nu>} \equiv 2 \nabla^{(\mu} u^{\nu)} - \frac{2}{3} \Delta^{\mu\nu} \nabla^\alpha u_\alpha \quad (\text{C1})$$

where

$$\nabla^{(\mu} u^{\nu)} = \frac{1}{2} (\nabla^\mu u^\nu + \nabla^\nu u^\mu) \quad (\text{C2})$$

and $\Delta^{\mu\nu} = g^{\mu\nu} - u^\mu u^\nu$, $\nabla^\mu = \partial^\mu - u^\mu D$.

Now $\nabla^{<0} u^0 >$ and $\nabla^{<z} u^z >$ can be defined as,

$$\nabla^{<0} u^0 > = 2 \nabla^0 u^0 - \frac{2}{3} (g^{00} - u^0 u^0) \nabla^\alpha u_\alpha \quad (\text{C3})$$

$$\nabla^{<z} u^z > = 2 \nabla^z u^z - \frac{2}{3} (g^{zz} - u^z u^z) \nabla^\alpha u_\alpha \quad (\text{C4})$$

Taking the difference of Eq. (C3) and Eq. (C4), we have

$$\begin{aligned} \nabla^{<0} u^0 > - \nabla^{<z} u^z > \\ = 2(\nabla^0 u^0 - \nabla^z u^z) - \frac{2}{3} (2 + \gamma^2 (v_z^2 - 1)) \nabla^\alpha u_\alpha \end{aligned} \quad (\text{C5})$$

Solving the Eq. (C5) in the limit $\eta \rightarrow 0$, finally we get;

$$\begin{aligned} \nabla^{<0} u^0 > - \nabla^{<z} u^z > = \frac{2\gamma}{\tau} \left[\gamma^4 \frac{\omega x}{2} \left(\frac{\omega^3 x^3}{8} + 1 \right) - 1 \right. \\ \left. - \frac{1}{3} \left(1 + \frac{\gamma^2 \omega^2 x^2}{4} \right)^2 - \frac{1}{6} (1 - \gamma^2) \left(\frac{\gamma^2 \omega^2 x^2}{2} + 2 \right) \right] \end{aligned} \quad (\text{C6})$$

Appendix D: Coupling vorticity with viscosity

Let's solve $\lambda \pi_\alpha^{(\mu} \omega^{\nu)\alpha}$

$$\pi_\alpha^{(\mu} \omega^{\nu)\alpha} = \frac{1}{2} (\pi_\alpha^\mu \omega^{\nu\alpha} + \pi_\alpha^\nu \omega^{\mu\alpha})$$

By using the relation

$$A^{(\mu} B^{\nu)} = \frac{1}{2} (A^\mu B^\nu + A^\nu B^\mu)$$

With the help of metric tensor, we get;

$$\pi_\alpha^{(\mu} \omega^{\nu)\alpha} = \frac{1}{2} (g_{\alpha\rho} \pi^{\rho\mu} \omega^{\nu\alpha} + g_{\alpha\sigma} \pi^{\sigma\nu} \omega^{\mu\alpha})$$

From Eq. (23), we have

$$\begin{aligned} D\pi^{\mu\nu} = & -\frac{1}{\tau_\pi} \pi^{\mu\nu} - \frac{1}{2\beta_2} \pi^{\mu\nu} \left[\beta_2 \theta + TD \left(\frac{\beta_2}{T} \right) \right] \\ & + \frac{1}{\beta_2} \nabla^{<\mu} u^{\nu>} + \lambda \pi_\alpha^{(\mu} \omega^{\nu)\alpha} \end{aligned} \quad (\text{D1})$$

For $\mu = 0$ and $\nu = 0$,

$$\begin{aligned} D\pi^{00} = & -\frac{1}{\tau_\pi} \pi^{00} - \frac{1}{2\beta_2} \pi^{00} \left[\beta_2 \theta + TD \left(\frac{\beta_2}{T} \right) \right] \\ & + \frac{1}{\beta_2} \nabla^{<0} u^0 > + \lambda \pi_\alpha^{(0} \omega^{0)\alpha} \end{aligned} \quad (\text{D2})$$

For $\mu = z$ and $\nu = z$, we have

$$\begin{aligned} D\pi^{zz} = & -\frac{1}{\tau_\pi} \pi^{zz} - \frac{1}{2\beta_2} \pi^{zz} \left[\beta_2 \theta + TD \left(\frac{\beta_2}{T} \right) \right] \\ & + \frac{1}{\beta_2} \nabla^{<z} u^z > + \lambda \pi_\alpha^{(z} \omega^{z)\alpha} \end{aligned} \quad (\text{D3})$$

Writing $D = \gamma \frac{d}{d\tau}$ and $\theta = \partial_\mu u^\mu$ and subtracting Eq. (D3) from Eq. (D2), we get;

$$\begin{aligned} \frac{d}{d\tau} (\pi^{00} - \pi^{zz}) = & -\frac{1}{\gamma \tau_\pi} (\pi^{00} - \pi^{zz}) - \frac{1}{2\gamma \beta_2} (\pi^{00} - \pi^{zz}) \\ & \times \left[\beta_2 \partial_\mu u^\mu + T \gamma \frac{d}{d\tau} \left(\frac{\beta_2}{T} \right) \right] + \frac{1}{\gamma \beta_2} (\nabla^{<0} u^0 > - \nabla^{<z} u^z >) \\ & + \frac{\lambda}{\gamma} (\pi_\alpha^{(0} \omega^{0)\alpha} - \pi_\alpha^{(z} \omega^{z)\alpha}) \end{aligned} \quad (\text{D4})$$

Choosing $\omega^{0z} = -\omega^{z0} = \frac{\omega}{T}$ and writing $\pi^{00} - \pi^{zz} = \Phi$, The last term of Eq. (D4) transformed as;

$$\begin{aligned} (\pi_\alpha^{(0} \omega^{0)\alpha} - \pi_\alpha^{(z} \omega^{z)\alpha}) &= (\pi^{00} \omega^{z0} - \pi^{zz} \omega^{0z}) \\ &= -\frac{\omega}{T} (\pi^{00} - \pi^{zz}) \\ &= -\frac{\omega \Phi}{T} \end{aligned} \quad (\text{D5})$$

Using second-order transport coefficient $\lambda = \frac{1}{\tau}$, $\tau_\pi = 2\eta\beta_2$, $\beta_2 = 3/4P$, $\eta = bT^3$, Eq. (29) extends to the following form;

$$\begin{aligned} \frac{d\Phi}{d\tau} = & -\frac{2aT\Phi}{3\gamma b} - \frac{\Phi}{2\gamma} \left(\partial_\mu u^\mu - \frac{5\gamma}{T} \frac{dT}{d\tau} \right) \\ & + \frac{4aT^4}{3\tau\gamma} \left(\nabla^{<0} u^{0>} - \nabla^{<z} u^{z>} \right) - \frac{\omega\Phi}{\gamma T\tau}. \end{aligned} \quad (\text{D6})$$

References

1. F. Becattini, F. Piccinini, J. Rizzo, Phys. Rev. C **77**, 024906 (2008)
2. L. Adamczyk, et al. (STAR Collaboration), Nature (London) **62**, 548 (2017)
3. B. Betz, M. Gyulassy, G. Torrieri, Phys. Rev. C **76**, 044901 (2007)
4. X.L. Xia, H. Li, Z.B. Tang, Q. Wang, Phys. Rev. C **98**, 024905 (2018)
5. Y. Jiang, Z.W. Lin, J. Liao, Phys. Rev. C **94**, 044910 (2016)
6. Y. Jiang, Z.W. Lin, J. Liao, Phys. Rev. C **95**, 049904(E) (2017)
7. D.X. Wei, W.T. Deng, X.G. Huang, Phys. Rev. C **99**, 014905 (2019)
8. F. Becattini, I. Karpenko, Phys. Rev. Lett. **120**, 012302 (2018)
9. L.G. Pang, H. Petersen, Q. Wang, X.N. Wang, Phys. Rev. Lett. **117**, 192301 (2016)
10. S.A. Voloshin, EPJ Web Conf. **171**, 07002 (2018)
11. A. Einstein, W.J. de Haas, Verh. Dtsch. Phys. Ges. **17**, 152 (1915)
12. S.J. Barnett, Phys. Rev. **6**, 239 (1915)
13. F. Becattini, G. Inghirami, V. Rolando, A. Beraudo, L. Del Zanna, A. De Pace, M. Nardi, G. Pagliara, V. Chandra, Eur. Phys. J. C **75**, 406 (2015)
14. F. Becattini, G. Inghirami, V. Rolando, A. Beraudo, L. Del Zanna, A. De Pace, M. Nardi, G. Pagliara and V. Chandra, **78**, 354(E) (2018)
15. L.P. Csnerai, V.K. Magas, D.J. Wang, Phys. Rev. C **87**, 034906 (2013)
16. L.P. Csnerai, D.J. Wang, M. Bleicher, H. Stöcker, Phys. Rev. C **90**, 021904 (2014)
17. Y.B. Ivanov, V.D. Toneev, A.A. Soldatov, Phys. Rev. C **100**, 014908 (2019)
18. I. Karpenko, F. Becattini, Eur. Phys. J. C **77**, 213 (2017)
19. W.T. Deng, X.G. Huang, Phys. Rev. C **93**, 064907 (2016)
20. H. Li, L.G. Pang, Q. Wang, X.L. Xia, Phys. Rev. C **96**, 054908 (2017)
21. X.G. Deng, X.G. Huang, Y.G. Ma, S. Zhang, Phys. Rev. C **101**, 064908 (2020)
22. O. Vitiuk, L.V. Bravina, E.E. Zabrodin, Phys. Lett. B **803**, 135298 (2020)
23. O. Rogachevsky, A. Sorin, O. Teryaev, Phys. Rev. C **82**, 054910 (2010)
24. D. Kharzeev, A. Zhitnitsky, Nucl. Phys. A **797**, 67 (2007)
25. D.E. Kharzeev, L.D. McLerran, H.J. Warringa, Nucl. Phys. A **803**, 227 (2008)
26. K. Fukushima, D.E. Kharzeev, H.J. Warringa, Phys. Rev. D **78**, 074033 (2008)
27. D.T. Son, A.R. Zhitnitsky, Phys. Rev. D **70**, 074018 (2004)
28. M.A. Metlitski, A.R. Zhitnitsky, Phys. Rev. D **72**, 045011 (2005)
29. N. Banerjee, J. Bhattacharya, S. Bhattacharyya, S. Dutta, R. Loganayagam, P. Surowka, JHEP **01**, 094 (2011)
30. J. Erdmenger, M. Haack, M. Kaminski, A. Yarom, JHEP **01**, 055 (2009)
31. D.T. Son, P. Surowka, Phys. Rev. Lett. **103**, 191601 (2009)
32. Y. Jiang, X.G. Huang, J. Liao, Phys. Rev. D **92**, 071501 (2015)
33. L.P. Csnerai, S. Velle, D.J. Wang, Phys. Rev. C **89**, 034916 (2014)
34. P. Kovtun, D.T. Son, A.O. Starinets, Phys. Rev. Lett. **94**, 111601 (2005)
35. J. Adams et al., STAR Collaboration, Nucl. Phys. A **757**, 102 (2005)
36. B. Fu, S.Y.F. Liu, L. Pang, H. Song, Y. Yin, Phys. Rev. Lett. **127**, 142301 (2021)
37. X.G. Huang, J. Liao, Q. Wang, X.L. Xia, arXiv:2010.08937 [nucl-th]
38. B. Singh, J.R. Bhatt, H. Mishra, Phys. Rev. D **100**, 014016 (2019)
39. A. Muronga, Phys. Rev. Lett. **88**, 062302 (2002)
40. A. Muronga, Phys. Rev. Lett. **89**, 159901(E) (2002)
41. A. Muronga, Phys. Rev. C **69**, 034903 (2004)
42. S. Weinberg, *Gravitation and Cosmology: Principles and Applications of the General Theory of Relativity* (Wiley, New York, 1972)
43. P. Romatschke, Int. J. Mod. Phys. E **19**, 53 (2010)
44. W. Florkowski, B. Friman, A. Jaiswal, E. Speranza, Phys. Rev. C **97**, 041901 (2018)
45. F. Becattini, L. Tinti, Ann. Phys. **325**, 1566 (2010)
46. H. Song, U.W. Heinz, Phys. Rev. C **78**, 024902 (2008)
47. V. Roy, S. Pu, L. Rezzolla, D. Rischke, Phys. Lett. B **750**, 45 (2015)
48. R. Biswas, A. Dash, N. Haque, S. Pu, V. Roy, JHEP **10**, 171 (2020)
49. S. Pu, V. Roy, L. Rezzolla, D.H. Rischke, Phys. Rev. D **93**, 074022 (2016)
50. C.R. Singh, S. Deb, R. Sahoo, J. Alam, Eur. Phys. J. C **82**, 542 (2022)